analytical chemistry

pubs.acs.org/ac Article

Simultaneous Monitoring of the Adenosine Triphosphate Levels in the Cytoplasm and Nucleus of a Single Cell with a Single Nanowire-Based Fluorescent Biosensor

Mingliang Mei, Lixuan Mu,* Yuan Wang, Sen Liang, Qiaowen Zhao, Lushan Huang, Guangwei She, and Wensheng Shi*

Cite This: *Anal. Chem.* 2022, 94, 11813−11820 Read Online

ACCESS | Metrics & More | Article Recommendations | Supporting Information

ABSTRACT: Simultaneous monitoring of the ATP levels at various sites of a single cell is crucial for revealing the ATP-related processes and diseases. In this work, we rationally fabricated single nanowire-based fluorescence biosensors, by which the ATP levels of the cytoplasm and nucleus in a single cell can be simultaneously monitored with a high spatial resolution. Utilizing the as-fabricated single nanowire biosensor, we demonstrated that the ATP levels of the cytoplasm were around 20−30% lower than that of the nucleus in both L929 and HeLa cells. Observing the ATP fluctuation of the cytoplasm and nucleus of the L929 and HeLa cells stimulated by Ca^{2+}, oligomycin, or under cisplatin-induced apoptosis, we found that the ATP levels at two cellular sites exhibited discriminative changes, revealing the different mechanisms of the ATP at these two cellular sites in response to the stimulations.

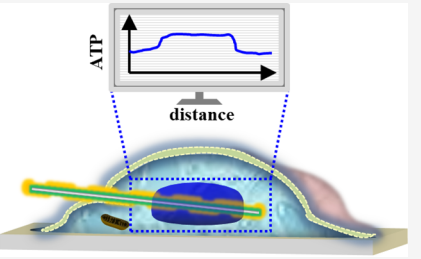

Adenosine triphosphate (ATP), also called "cellular energy currency", plays a pivotal role in various cellular events, including cell divisions, enzyme reactions, protein synthesis, etc.[1−4] The cellular events that were differently active and took place at various cellular sites would differentially influence the ATP levels from site to site and organelle to organelle. Detecting the ATP levels at the different sites or organelles, in turn, would be of benefit to portend or further regulate the cellular events for screening, diagnosis, and treatment of the diseases.[5,6] For example, the ATP level around the cell membrane was utilized to evaluate the activity of the exocytosis and cell signaling.[7,8] The ATP level of the mitochondria would link with the start of the cell apoptosis.[9,10] Meanwhile, a disorder of ATP levels was found in the Alzheimer's and Parkinson's disease-related cells.[11] However, due to the scarcity of ATP biosensors with high spatial resolution in cells, it is difficult to comprehensively understand the cellular events from the ATP level and clearly demonstrate the correlation between the pathogenesis of these diseases and the ATP levels of the cells. Therefore, to accurately and simultaneously monitor the ATP levels at various sites of the cells is a key issue for elucidation of cellular events or pathogenesis.

To date, numerous ATP biosensors have been fabricated for monitoring cellular ATP levels.[12,13] However, most of the reported ATP biosensors for cells were made of zero-dimensional (0D) nanomaterials or small molecules.[14,15] The Brownian motions of the 0D nano-materials or the random thermal motion of small molecules would induce an unceasing movement of the ATP biosensors in the living cell. As a result, the spatial resolution of the ATP biosensors would be reduced, and the signal from the biosensors for a specific cellular site does not veritably and accurately reveal the ATP level at that position.[16,17] Making an ATP biosensor with a targeting unit is a fine approach to improve the spatial resolution of the biosensor. However, the ATP biosensor with a targeting unit could only determine the ATP level of the specific organelle anchored by the targeting unit.[13,15,18] Given that the ATP-related processes were always involved in many cellular sites simultaneously, to detect the ATP level in only one organelle is not enough to comprehensively demonstrate the whole ATP-related processes.[19,20] Hence, especially essential are ATP biosensors, which not only possess a high spatial resolution but also could simultaneously monitor the ATP levels at various cellular sites.

As an alternative strategy, the sensitive units can be decorated onto one dimensional (1D) nano-materials to construct the 1D-based biosensors for monitoring the analyte with an excellent spatial resolution by which the Brownian motions of the sensors could be restrained.[21,22] For instance, Li's group designed an ingenious single-cell thermometer by encapsulating upconversion nanoparticles into spider silks.

Received: May 10, 2022
Accepted: July 25, 2022
Published: August 4, 2022

https://doi.org/10.1021/acs.analchem.2c02030
Anal. Chem. 2022, 94, 11813−11820

Owing to the microscale length of the spider silks, the thermometer barely moved during the sensing process, which therefore was able to monitor the temperature at various positions of the cells with a high spatial resolution.[23] Our group also reported some 1D biosensors based on silicon nanowires, which can be purposefully inserted into cellular sites under the help of a micromanipulator. Also, the bioanalyte in cells can be accurately sensed.[24,25] Considering the advantage of the 1D biosensors in spatial resolution, we designed a silicon nanowire-based fluorescent biosensor to monitor cellular ATP levels with a high spatial resolution, in which the silicon nanowires (SiNWs) were selected as the substrate while the *N*-(rhodamine-B)-lactam-1, 2-diethylenetriamine (Rho-N_3H_5), and fluorescein isothiocyanate (FITC) were selected as the ATP-sensitive units.[26,27] As shown in Scheme 1, the SiNWs were first encapsulated by a SiO_2 layer

Scheme 1. Design of the SiNWs-FITC@SiO_2-Rho and Illustration of the SiNWs-FITC@SiO_2-Rho for the ATP Sensing in a Single Cell with a High Spatial Resolution

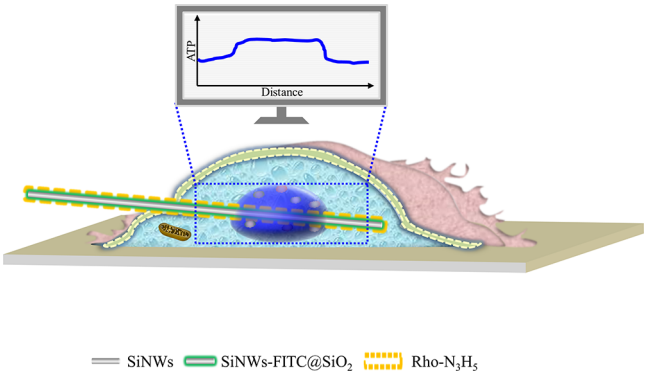

containing FITC to form SiNWs-FITC@SiO_2. The surface of the SiNWs-FITC@SiO_2 was subsequently modified by a carboxyl-terminal siloxane reagent (SiNWs-FITC@SiO_2-COOH). Hence, the Rho-N_3H_5 molecules with an NH_2-terminal can be grafted on the surface of the SiNWs-FITC@SiO_2-COOH through an EDC/NHSS chemistry to finally form the SiNW-based fluorescent biosensors (SiNWs-FITC@SiO_2-Rho) for ATP. The SiNWs-FITC@SiO_2-Rho performed a ratiometric response of the emissions from Rho-N_3H_5 and FITC to ATP. Moreover, the SiNWs-FITC@SiO_2-Rho exhibited a fine photo-stability, which is essential to investigate ATP-related cellular events for a long time.

Considering the importance of the cytoplasm and nucleus in living cells, we utilized the SiNWs-FITC@SiO_2-Rho to simultaneously monitor the ATP levels at these two intracellular sites of a single L929 and HeLa cell. It was found that the ATP level of the cytoplasm was around 20−30% lower than that of the nucleus, and the ATP levels of the cytoplasm decreased as the detecting sites got away from the nucleus in most cases. Moreover, the ATP in the cytoplasm and nucleus of the L929 and HeLa cells stimulated by Ca^{2+} or oligomycin exhibited discriminative responses. We further investigated the ATP fluctuation of the cytoplasm and nucleus during the apoptosis of the L929 and HeLa cells induced by cisplatin and accordingly revealed the different roles of ATP in the cytoplasm and nucleus in response to the apoptosis. The ATP biosensors developed in this work can be utilized to simultaneously monitor the ATP in more intracellular sites with a high spatial resolution. Moreover, apart from observing the apoptosis, the as-prepared ATP biosensor could be anticipated for the investigation of more ATP-related cellular events.

EXPERIMENTAL SECTION

Materials and Instruments. The materials and instruments used are listed in detail in the Supporting Information.

Synthesis of the Rho-N_3H_5, SiNWs, SiNWs-FITC@SiO_2, and SiNWs-FITC@SiO_2-Rho. The Rho-N_3H_5 was synthesized according to the previous report with a little modification, and the detailed process is presented in the Supporting Information (Supporting Information, method 1).[26] The final product was a deep orange solid with a yield of 30%. ^{1}H NMR (Figure S1) (400 MHz, $CDCl_3$): δ 7.90 (m, 1H), 7.44 (m, 2H), 7.09 (m, 1H), 6.43 (m, J = 8.70 Hz, 2H), 6.38 (s, 2H), 6.27 (d, J = 8.60 Hz, 2H) 3.34−3.27 (m, 10H), 2.61 (t, J = 5.7 Hz, 2H), 2.46−2.41 (m, 4H), 1.60−1.40 (br, s), 1.16 (t, J = 6.40 Hz, 12H). MS (Figure S2, m/*z*) 528.3. The SiNWs, SiNWs-FITC@SiO_2, and SiNWs-FITC@SiO_2-Rho were fabricated referring to our previous work (Supporting Information, methods 2 and 3).[24,25]

Fluorescence Imaging of the SiNWs-FITC@SiO_2-Rho. A 20 μL SiNWs-FITC@SiO_2-Rho stock solution was added into 480 μL 1 × PBS in a confocal dish for observation under a Nikon A1 laser scanning confocal microscope. A 488 nm laser and a 561 nm laser were employed to excite the FITC and Rho-N_3H_5, respectively. The green fluorescence of FITC was collected from 500 to 550 nm (I_g), while the orange fluorescence of Rho-N_3H_5 was collected from 570 to 620 nm (I_o). The detailed optimization and sensing properties of the SiNWs-FITC@SiO_2-Rho are described in the Supporting Information (method 4: optimization of the SiNWs-FITC@SiO_2-Rho; methods 5−10: the uniformity, response times, calibration curves, selectivity, photo/pH/polarity-stability, and reversibility of the SiNWs-FITC@SiO_2-Rho to ATP).

Determination of the ATP Levels through the Calibration Curve. The ATP levels were determined according to the Supporting Information, method 11. For the determination of the ATP levels of the nucleus and cytoplasm, the part of the SiNWs-FITC@SiO_2−20-Rho-100 located in the nucleus and cytoplasm was selected to calculate the ATP levels of the nucleus and cytoplasm.

Monitoring the ATP Fluctuation in Living Cells. Briefly, the SiNWs-FITC@SiO_2-20-Rho-100 was added to the cell culture medium and incubated with the living cells for around 3 days. Before the observation, the cells were first stained with Hoechst 33342 (10 μL, 1 mg/mL). Then, the cells were washed carefully with 1× PBS three times. 5 mM Ca^{2+}, 10 μM oligomycin, and 50 μM cisplatin were employed to change the ATP levels of the living cells. The detailed experimental processes are described in the Supporting Information, methods 12 and 13.

RESULTS AND DISCUSSIONS

Improvement of the Ratiometric Response of the SiNWs-FITC@SiO_2-Rho to ATP. As ATP can activate the fluorescence of Rho-N_3H_5 and quench the fluorescence of FITC,[26,27] the amounts of Rho-N_3H_5 and FITC decorated on the SiNWs-FITC@SiO_2-Rho would regulate the ratiometric response of the SiNWs-FITC@SiO_2-Rho to ATP. Hence, the volume of the FITC-APTES conjugate and the concentrations

https://doi.org/10.1021/acs.analchem.2c02030
Anal. Chem. 2022, 94, 11813−11820

of the Rho-N_3H_5 used for preparing the SiNWs-FITC@SiO_2-Rho were carefully adjusted to improve the response of the ATP biosensors to ATP, and the corresponding products were defined as SiNWs-FITC@SiO_2-a-Rho-b (a/μL represents the volume of the FITC-APTES conjugate, while b/μM represents the concentration of the Rho-N_3H_5). First, the responses of the SiNWs-FITC@SiO_2-0-Rho-20 and the SiNWs-FITC@SiO_2-20-Rho-0 to ATP were examined, and the results are shown in Figure S3. ATP can increase the fluorescence of the Rho-N_3H_5 moiety of the SiNWs-FITC@SiO_2-0-Rho-20 (Figure S3a) and quench the fluorescence of the FITC moiety of the SiNWs-FITC@SiO_2-20-Rho-0 (Figure S3b). To determine the suitable volume of the FITC-ATPES conjugate, the concentration of the Rho-N_3H_5 was fixed at 20 μM initially. Five different samples including SiNWs-FITC@SiO_2-5/10/20/40/80-Rho-20 were prepared. The dependence of the intensity ratios (I_o/I_g, I_o represents the fluorescence intensity of the Rho-N_3H_5 moiety, while the I_g represents the fluorescence intensity of the FITC moiety) of the SiNWs-FITC@SiO_2-a-Rho-20 with 10 mM ATP on the volume of the FITC-APTES conjugate were examined, and the results are shown in Figure S4a. The I_o/I_g of the SiNWs-FITC@SiO_2-a-Rho-20 gradually increased with the increase of the FITC-APTES conjugate and reached a plateau as the volume of the FITC-APTES conjugate reached 20 μL. Hence, the FITC-APTES conjugate of 20 μL was employed in the following improvements. To determine the appropriate concentrations of the Rho-N_3H_5, the Rho-N_3H_5 with concentrations of 20/40/60/100/200/400/500 μM were selected. The I_o/I_g of the SiNWs-FITC@SiO_2-20-Rho-b gradually increased with the increase of the Rho-N_3H_5 and reached a plateau at 100 μM Rho-N_3H_5 (10 mM ATP, Figure S4b). Accordingly, the SiNWs-FITC@SiO_2-20-Rho-100 was used as the SiNW-based ATP biosensors for the following experiments.

Characterizations of the SiNWs, SiNWs-FITC@SiO_2-20, and SiNWs-FITC@SiO_2-20-Rho-100. The morphology of the SiNWs was characterized by a scanning electron microscope and transmission electron microscope (Figure S5 and Figure S6), from which the average length and diameter of the SiNWs were determined to be 72.9 $\pm$ 2.6 μm and 278 nm $\pm$ 86 nm, respectively. Moreover, a straight structure and smooth surface were observed from the SiNWs (Figure S6). However, the surface of the SiNWs-FITC@SiO_2 was coarse due to the formation of the FITC@SiO_2 layer on the surface of the SiNWs after the modification of the FITC-APTES and TEOS. A smoother surface was observed from the SiNWs-FITC@SiO_2-20-Rho-100. The difference between the surface roughness of the SiNWs-FITC@SiO_2-20 and SiNWs-FITC@SiO_2-20-Rho-100 could be ascribed to the different reaction rates of silane reagents used in the synthetic processes.[28] XPS measurements were performed for determining the surface compositions of the SiNWs, SiNWs-FITC@SiO_2-20, and SiNWs-FITC@SiO_2-20-Rho-100. The high-resolution spectra of Si 2p and N 1s of the three samples are shown in Figure S7. An intense peak corresponding to bulk Si (99 eV) and a moderated peak corresponding to silicon oxide (103 eV) were observed from the SiNWs.[29,30] For the SiNWs-FITC@SiO_2-20, the peak from the bulk silicon disappeared and the peak from the silicon oxide still existed (Figure S7a). A new intense peak corresponding to the −NH−C(*S*)−NH− (400.6 eV) appeared,[31] indicating the formation of the FITC@SiO_2 layer on the SiNWs (Figure S7b). After the decoration of the carboxyl-terminal siloxane reagents and Rho-N_3H_5, intense peaks corresponding to $-N(C_2H_5)_2$ (399.5 eV) and −C(O)−NH− (401.6 eV) were observed from the SiNWs-FITC@SiO_2-20-Rho-100,[32,33] demonstrating the successful modification of the SiNWs-FITC@SiO_2-20 by the Rho-N_3H_5. Furthermore, the fluorescence from the SiNWs, SiNWs-FITC@SiO_2-20, and SiNWs-FITC@SiO_2-20-Rho-100 were investigated by a laser scanning confocal microscope. At the same experimental conditions, the bright green fluorescence of the FITC moiety and orange fluorescence of the Rho-N_3H_5 moiety were observed from the SiNWs-FITC@SiO_2-20-Rho-100, while only green fluorescence can be found from the SiNWs-FITC@SiO_2-20, and no fluorescence was detected from the SiNWs (Figure S8). These results further demonstrated that the FITC and Rho-N_3H_5 moieties have been successfully decorated onto the surface of the SiNWs.

Uniformity of the SiNWs-FITC@SiO_2-20-Rho-100. The uniformity of the SiNWs-FITC@SiO_2-20-Rho-100 is critical for accurately monitoring the ATP levels in a high spatial resolution. Therefore, the confocal images of eight different samples fetched from the same batch were recorded by a laser scanning confocal microscope, and the uniformity of the samples was examined. The ratiometric images were obtained through calculating the intensity ratio of the Rho-N_3H_5 moiety to the FITC moiety (Supporting Information, method 5). It can be observed that the color of the ratiometric images was uniform (Figure S9a−d). The I_o/I_g values at different points of the SiNWs-FITC@SiO_2-20-Rho-100 were close (Figure S9e). Moreover, no obvious dispersion of the I_o/I_g was observed from these eight samples (Figure S9f). These results demonstrated that the SiNWs-FITC@SiO_2-20-Rho-100 is uniform, and there is little differentiation between the various SiNWs-FITC@SiO_2-20-Rho-100 fetched from the same batch, which ensured an accurate measurement for the ATP.

Sensing Properties of the SiNWs-FITC@SiO_2-20-Rho-100 to ATP. The response times of the SiNWs-FITC@SiO_2-20-Rho-100 for ATP detection were investigated (Supporting Information, method 6). The response of the SiNWs-FITC@SiO_2-20-Rho-100 to 2 mM ATP was around 8 min. When the ATP concentration was increased from 2 to 4 and 8 mM, the response times extended to 10 and 13 min, respectively (Figure S10), which is swift enough to monitor the ATP fluctuation during a cellular event.[5,15] Furthermore, the confocal images of the SiNWs-FITC@SiO_2-20-Rho-100 treated with ATP with different concentrations were collected, and the results are shown in Figure 1a (three parallel samples in Figure S11). With the continuous addition of ATP, the green fluorescence of the SiNWs-FITC@SiO_2-20-Rho-100 gradually faded, while the orange fluorescence brightened. The spectral responses of the SiNWs-FITC@SiO_2-20-Rho-100 to ATP are also presented in the Supporting Information (Figure S12). The I_o/I_g values at the points along the axial direction of the SiNWs-FITC@SiO_2-20-Rho-100 were calculated and recorded automatically by the laser scanning confocal microscope. The average and the error bar of the I_o/I_g were determined from the I_o/I_g at these points. The average I_o/I_g of the SiNWs-FITC@SiO_2-20-Rho-100 increased from around 0.2 to around 4.6 with the increase of ATP from 0 to 10 mM with an interval of 2 mM, revealing a fine ratiometric response of the SiNWs-FITC@SiO_2-20-Rho-100 to ATP (Figure 1b, black dots; Supporting Information, method 7). The calibration curve was obtained by plotting the ratiometric responses (I_o/I_g) of the SiNWs-FITC@SiO_2-20-Rho-100 against ATP concentrations and fitted with a logistic equation

https://doi.org/10.1021/acs.analchem.2c02030
Anal. Chem. 2022, 94, 11813−11820

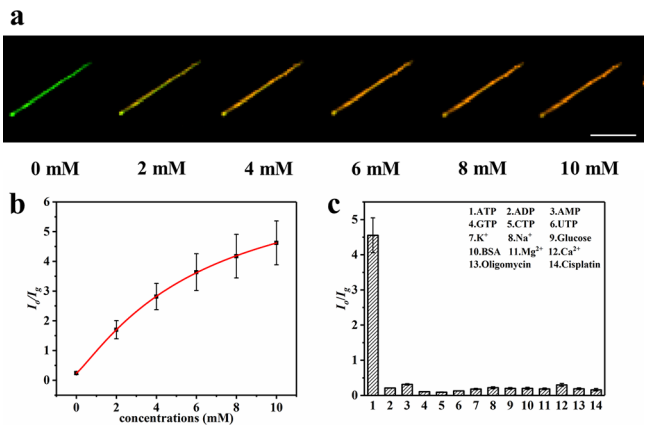

Figure 1. (a) Confocal images of the SiNWs-FITC@SiO_2-20-Rho-100 treated with ATP (0−10 mM, scale bar: 10 μm). (b) Calibration curve of the SiNWs-FITC@SiO_2-20-Rho-100 in response to concentrations of ATP (the red curve was the fitting curve; the error bar was determined from the I_o/I_g at the points ($n \geq 65$ points on the single sensor) along the axial direction of the SiNWs-FITC@SiO_2-20-Rho-100; error bars represent standard deviation). (c) Selectivity of the SiNWs-FITC@SiO_2-20-Rho-100 to ATP (ATP, ADP, AMP, glucose = 10 mM; GTP, CTP, UTP, Mg^{2+} = 2 mM; K^+, Na^+ = 100 mM; BSA, oligomycin = 10 μM; Ca^{2+} = 5 mM; cisplatin = 50 μM, n = 3, error bars represent standard deviation).

(Figure 1b, red line), which can be used in the following experiments to determine the concentration of the ATP according to the result of I_o/I_g.

The selectivity of the SiNWs-FITC@SiO_2-20-Rho-100 to ATP was evaluated (Supporting Information, method 8). As shown in Figure 1c, only the ATP of 10 mM can notably increase the I_o/I_g of the SiNWs-FITC@SiO_2-20-Rho-100, while no obvious changes were observed as the samples were treated with ADP (10 mM), AMP (10 mM), CTP (2 mM), UTP (2 mM), GTP (2 mM), Mg^{2+} (2 mM), Ca^{2+} (5 mM), K^+ (100 mM), Na^+ (100 mM), glucose (10 mM), BSA (10 μM), oligomycin (10 μM), or cisplatin (50 μM), respectively. The above results evidenced that the SiNWs-FITC@SiO_2-20-Rho-100 had an outstanding selectivity for ATP.

The photostability of the SiNWs-FITC@SiO_2-20-Rho-100 in the presence of 4 mM ATP was examined (Supporting Information, method 9). As shown in Figure S13, the I_o/I_g of the SiNWs-FITC@SiO_2-20-Rho-100 was stable even though the sample was continuously exposed to intense lasers (488 nm, 8 μW; 561 nm, 14 μW) for 10 min, being suitable to monitor the cellular events for a long time. Moreover, as the FITC moiety was pH- and polarity-sensitive, the responses of the SiNWs-FITC@SiO_2-20-Rho-100 treated with 4 mM ATP were examined under different pH values and polarities (Supporting information, Figure S14, method 9). It was observed that the SiNWs-FITC@SiO_2-20-Rho-100 exhibited good pH stability in the range of 7.1−7.9 and good polarity stability, which can well rule out the signal changes of the sensor caused by the changes in the cell microenvironment.[34−37]

Switching the ATP concentrations between 2 and 4 mM (Figure 2a, Supporting Information, method 10), we can find a reversible change of the I_o/I_g of the SiNWs-FITC@SiO_2-20-Rho-100 (Figure 2b, black dotted line) and the ATP levels determined from the I_o/I_g and calibration curves (Figure 2b, red dotted line; Supporting Information, method 11). It indicated that the SiNWs-FITC@SiO_2-20-Rho-100 had an

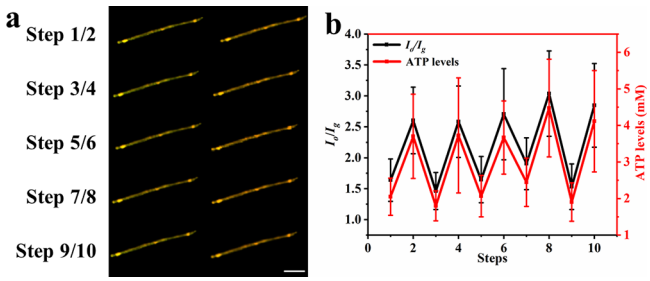

Figure 2. (a) Confocal images of the SiNWs-FITC@SiO_2-20-Rho-100 treated with 2 and 4 mM ATP repeatedly (in steps 1, 3, 5, 7, and 9, the ATP level was 2 mM, while the ATP level was 4 mM in the other steps, scale bar: 10 μm). (b) Average I_o/I_g (black dotted line) of the SiNWs-FITC@SiO_2-20-Rho-100 and ATP level (red dotted line) at each step (the error bars of I_o/I_g and ATP levels were determined from the I_o/I_g and ATP levels at the points ($n \geq 80$ points on a single sensor) along the axial direction of the SiNWs-FITC@SiO_2-20-Rho-100; error bars represent standard deviation).

excellent reversibility in detecting ATP. Accordingly, the SiNWs-FITC@SiO_2-20-Rho-100 as an excellent ATP biosensor was qualified to monitor ATP levels in living cells.

Determination of the ATP Distribution in Living Cells. Two types of cells including L929 and HeLa cells were incubated with the SiNWs-FITC@SiO_2-20-Rho-100. The cell experiments were carried out according to the processes presented in the Supporting Information, method 12. As shown in Figure S15, owing to the existence of ATP in living cells, the Rho-N_3H_5 moiety on the SiNWs-FITC@SiO_2-20-Rho-100 that was incubated across the cells can be activated by the ATP and an orange fluorescence was emitted, while the green fluorescence from the FITC was quenched by the ATP. Thereby, the SiNWs-FITC@SiO_2-20-Rho-100 located inside the living cell showed mainly a strong orange fluorescence (Figure S15a,b). In the same experimental condition, the Rho-N_3H_5 on the SiNWs-FITC@SiO_2-20-Rho-100 cannot be activated by little ATP existing in the cell culture medium. As a result, the SiNWs-FITC@SiO_2-20-Rho-100 located outside of the cell showed mainly a green fluorescence emitted from the FITC (Figure S15c,d). Accordingly, it can be rational to differentiate between the SiNWs-FITC@SiO_2-20-Rho-100 located inside and outside of the living cell. Moreover, the positions of the SiNWs-FITC@SiO_2-20-Rho-100 and nucleus can also be determined by observing the fluorescence of the SiNWs-FITC@SiO_2-20-Rho-100 and Hoechst 33342 (Figure S16 and Movie S1). The different layers of a 3D image of a cell from *Z*-axis scanning are presented in Figure S16. It can be found that only the SiNWs-FITC@SiO_2-20-Rho-100 and nucleus were in the same layer; we could discern the SiNWs-FITC@SiO_2-20-Rho-100 and nucleus at the same time, which demonstrated that the nanowire was in the nucleus.

The ATP levels of the cytoplasm and nucleus in a single L929 cell were investigated through penetrating the nucleus with the SiNWs-FITC@SiO_2-20-Rho-100. To clearly observe the cell, the nucleus was blue-stained by Hoechst 33342 before observation and the cell outline is represented by a white dashed line (Figure 3a,b). In Figure 3a, the intersections between the SiNWs-FITC@SiO_2-20-Rho-100 and the boundary of the nucleus were marked with point 2, which corresponded to point 2 in Figure 3c. We can find that the points between point 1 and point 2 were in the nucleus and the

https://doi.org/10.1021/acs.analchem.2c02030
Anal. Chem. 2022, 94, 11813−11820

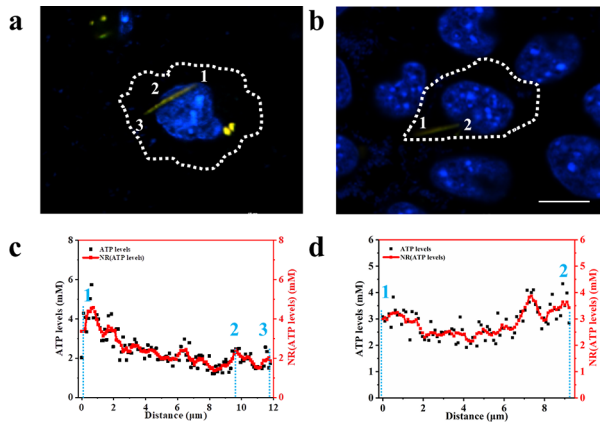

Figure 3. (a) Confocal image of the SiNWs-FITC@SiO_2-20-Rho-100, which penetrated through the nucleus. (b) Confocal image of the SiNWs-FITC@SiO_2-20-Rho-100, which is located in the cytoplasm (scale bar: 10 μm). (c) ATP levels determined by the SiNWs-FITC@SiO_2-20-Rho-100 shown in (a) (points 1, 2, and 3 in (c) correspond to points 1, 2, and 3 in (a)). (d) ATP levels determined by the SiNWs-FITC@SiO_2-20-Rho-100 shown in (b) (points 1 and 2 in (d) corresponde to points 1 and 2 in (b)) (the black dots in (c) and (d) are the calculated ATP levels, while the red lines in (c) and (d) are the trend lines of the ATP level along the axial direction of the SiNWs-FITC@SiO_2-20-Rho-100 shown in (a) and (b)).

points between 2 and 3 were in the cytoplasm. Measuring the I_o/I_g from the confocal images of the SiNWs-FITC@SiO_2-20-Rho-100 and employing the calibration curve, we can determine the ATP concentrations at the points along the axial direction of the SiNWs-FITC@SiO_2-20-Rho-100 (Figure 3c, black dots). To clearly observe the distribution tendency of the ATP levels, a trend line of the ATP level along the SiNWs-FITC@SiO_2-20-Rho-100 was drawn as the red line in Figure 3c (Supporting Information, method 11). Observing the ATP levels along SiNWs-FITC@SiO_2-20-Rho-100, we can find that the ATP levels of most points located between point 2 and point 3 were lower than that of the points located between point 1 and 2, especially the ATP levels at the points around point 1 (distance from 0 to 6 μm). However, we also found that the ATP levels of some points located between point 2 and point 3 were not lower than some points located between point 1 and point 2. It seemed that the ATP level of the cytoplasm was lower than that of the nucleus. Furthermore, we averaged ATP levels at the points located in the cytoplasm and nucleus. The ATP level of the cytoplasm and nucleus were 1.9 ± 0.4 (20 points) and 2.5 ± 0.9 mM (95 points) determined from the observed cell, in which the error bars were determined from the ATP levels at the points located in the cytoplasm and nucleus, respectively. Clearly, even though the ATP levels of some points in the cytoplasm were higher than that in the nucleus, the average ATP levels of the cytoplasm were lower than that of the nucleus ($P < 10^{-5}$, Student's t-test). Observing the 14 parallel samples (Figure S17a), we found that the ATP level of the cytoplasm was 21 ± 8% lower than that of the nucleus ($n = 14$, $P < 0.05$, Student's t-test), which was consistent with the previous reports.[38] More interestingly, it seemed that the ATP levels slowly decreased from point 2 (2.5 mM) to point 3 (1.7 mM) in Figure 3c, implying a lower ATP level at the site away from the nucleus than that at the site near the nucleus. To confirm this point, the SiNWs-FITC@SiO_2-20-Rho-100 with a terminal close to the nucleus was selected. Two points at the SiNWs-FITC@SiO_2-20-Rho-100 located at the cytoplasm were marked with points 1 and 2 in Figure 3b, which correspond to points 1 and 2 in Figure 3d, respectively. Meanwhile, the trend line of the ATP level along the SiNWs-FITC@SiO_2-20-Rho-100 was also drawn as the red line in Figure 3d. As shown in Figure 3b,d, although there was a slight increase in the ATP levels at the sites near the cytomembrane (around point 1), the ATP level near the nucleus (around point 2) was still higher than that away from the nucleus (from point 2 to point 1). It is known that the endoplasmic reticulum is located mainly around the nucleus and is an important organelle to support many cellular events.[4] Therefore, more ATP has to be responsible to provide the energy for realizing the function of the endoplasmic reticulum. This may be why the ATP levels are higher around the nucleus. Likewise, the ATP levels of the cytoplasm of the HeLa cells were determined to be around 32 ± 18% ($n = 11$, $P < 0.05$, Student's t-test) lower than that of the nucleus (Figure S17b). The above results demonstrated that the SiNWs-FITC@SiO_2-20-Rho-100 is a powerful tool to simultaneously detect the ATP levels of the nucleus and cytoplasm with a high spatial resolution.

Real-Time Monitoring of the ATP Dependence of Living Cells on the Stimulation of Ca^{2+} and Oligomycin. The SiNWs-FITC@SiO_2-20-Rho-100 was employed to monitor the dependence of the ATP inside L929 and HeLa cells under the stimulation of Ca^{2+} and oligomycin. According to the previous reports, Ca^{2+} can promote ATP production; contrariwise, oligomycin can inhibit ATP production.[39] The pH changes of the L929 cells treated with Ca^{2+} and oligomycin were first evaluated by using a commercial pH sensor (BCECF AM). As shown in Figure S18 (Supporting Information, method 13), no obvious changes in the fluorescence of the BCECF AM were observed, suggesting that the pH changes of the cells treated with Ca^{2+} and oligomycin were negligible, which would not affect the signal of the sensor. The ATP levels of the cytoplasm and nucleus of the cells were high-spatially and simultaneously monitored in real-time when 5 mM Ca^{2+} or 10 μM oligomycin was added into the cell culture medium (Supporting Information, method 13). As shown in the confocal images (Figure 4a,b), the fluorescence of the SiNWs-FITC@SiO_2-20-Rho-100 that was incubated across the L929 cell turned from light green to orange after the cell was incubated with 5 mM Ca^{2+}. Meanwhile, in the ratiometric images (Figure 4c,d), the color of most points on the SiNWs-FITC@SiO_2-20-Rho-100 turned from blue to cyan, suggesting the increase of I_o/I_g at these points. According to the I_o/I_g and the calibration curve, we can find that the ATP levels of the cytoplasm and nucleus all increased with time and reached a plateau within 5 min (Figure 4e). Among them, the ATP levels of the nucleus and the cytoplasm increased from around 1.3 ± 0.2 and 1.1 ± 0.2 mM to 1.8 ± 0.3 and 1.7 ± 0.4 mM, respectively, after the treatment of Ca^{2+} for 5 min (Figure 4f). Ca^{2+}-induced ATP increments of 38 and 55% were exhibited in the nucleus and cytoplasm, respectively. Two more parallel experiments were performed, and the results presented in Table S1 also supported the above observation. Clearly, the increment in the ATP level of the cytoplasm was higher than that of the nucleus after the L929 cells were treated with Ca^{2+} of 5 mM, which might link with the mitochondria. It has been reported that Ca^{2+} can promote ATP production in the mitochondria,[40] which only existed in the cytoplasm. Therefore, the Ca^{2+}-induced increase of ATP in the mitochondria would elevate the ATP in the whole cytoplasm. Despite the lack of mitochondria in the nucleus, the ATP level of the

https://doi.org/10.1021/acs.analchem.2c02030
Anal. Chem. 2022, 94, 11813−11820

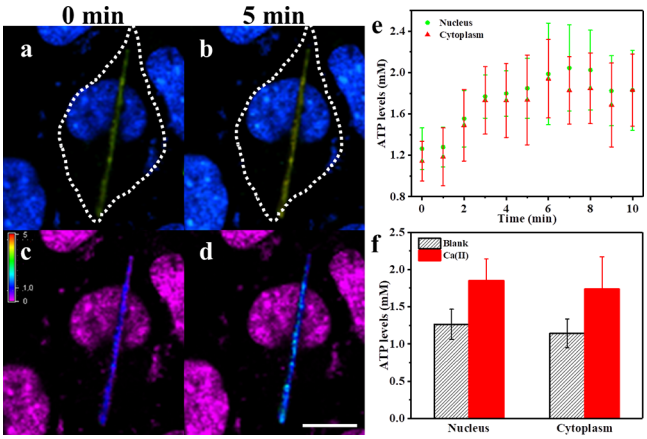

Figure 4. (a, b) Confocal images of the SiNWs-FITC@SiO_2-20-Rho-100 inside a single L929 cell treated (a) without and (b) with 5 mM Ca^{2+} for 5 min. (c, d) Ratiometric images of the SiNWs-FITC@SiO_2-20-Rho-100 inside a single L929 cell treated (c) without and (d) with 5 mM Ca^{2+} for 5 min (scale bar = 10 μm, ratio bar: 0−5). (e) Changes in the ATP levels of the nucleus (green dots, n = 25 points on the single sensor) and cytoplasm (red dots, n = 37 points on the single sensor) over time with an interval of 1 min. (f) ATP levels of the nucleus and cytoplasm in the absence (stripe bars) and presence of 5 mM Ca^{2+} (5 min, red bars) (the error bars represent the standard deviations based on the ATP levels at the points located in the cytoplasm and nucleus).

nucleus could be slowly elevated due to the diffusion of the ATP from the cytoplasm to the nucleus. Moreover, a similar dependence of the ATP fluctuation on the Ca^{2+} stimulation was also observed from the Ca^{2+}-stimulated HeLa cells (Figure S19).

Observing the ratiometric images of the L929 cells treated with oligomycin, we can find that the color of most points on the SiNWs-FITC@SiO_2-20-Rho-100 turned from green to deep blue as the continuation of the treatment (Figure 5a), indicating the decrease of the ATP levels at these points.

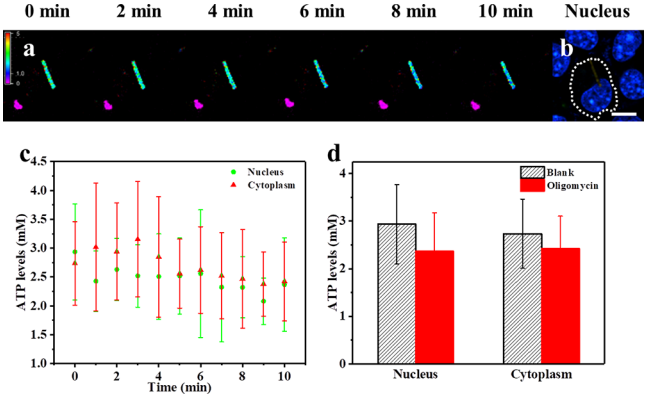

Figure 5. (a) Ratiometric images of the SiNWs-FITC@SiO_2-20-Rho-100 inside a single L929 cell treated with oligomycin (10 μM) for various times and (b) confocal image of the SiNWs-FITC@SiO_2-20-Rho-100 inside a single L929 cell (scale bar: 10 μm; ratio bar: 0−5). (c) ATP changes in the nucleus (green dots, n = 9 points on the single sensor) and cytoplasm (red dots, n = 18 points on the single sensor) over time in (a). (d) ATP levels of the nucleus and cytoplasm in the absence (stripe bars) and presence of 10 μM oligomycin (10 min, red bars) (the error bars represent the standard deviations based on the ATP levels at the points located in the cytoplasm and nucleus).

Combined with the confocal images, the ATP levels of the nucleus and cytoplasm can be determined (Figure 5b). It was found that the ATP levels of the nucleus (Figure 5c, green dots) and cytoplasm (Figure 5c, red dots) all decreased with time and reached a plateau within 10 min. Comparing the ATP levels of the nucleus and cytoplasm before and after the treatment (Figure 5d), we can determine that the ATP decrements of 17 and 11% were induced by the treatment of the oligomycin in the nucleus and cytoplasm, respectively. Two more parallel experiments were performed, and the results presented in Table S2 also propped up the above observation. Obviously, the treatment of the oligomycin could decrease the ATP level of the nucleus more than that of the cytoplasm. A similar phenomenon was also observed in the oligomycin-treated HeLa cells (Figure S20). The response of the nucleus and cytoplasm to oligomycin may be related to the "self-protection" of the cell itself.[41] It is known that the replication and transcription of DNA occurred in the nucleus and is associated with cell multiplication. Meanwhile, the cytoplasm was the main place to maintain the cell's life, such as cell signaling, protein synthesis, and enzymatic reactions.[3] When the cells were stimulated by the oligomycin, the ATP production in the cell was inhibited, which would result in a shortage of ATP. In this state, the scarce ATP was primarily used to maintain the cell's basic life supported by the cytoplasm, and the cell multiplication dominated by the nucleus had to be suspended. As a result, the decrement in the ATP level of the nucleus was more obvious.

The above investigation for the ATP dependence of the nucleus and cytoplasm in L929 and HeLa cells on the treatment of the Ca^{2+} and oligomycin verified that the SiNWs-FITC@SiO_2-20-Rho-100 was qualified to simultaneously monitor the ATP of the nucleus and cytoplasm of the cells under the stimulation.

Real-Time Monitoring of the ATP Fluctuation during Cell Apoptosis. The ATP fluctuation was monitored in real-time by the SiNWs-FITC@SiO_2-20-Rho-100 during the cell apoptosis. The cell apoptosis was induced by 50 μM cisplatin (Supporting Information, method 13),[42] which interacted with the DNA strand and affected the DNA functions such as transcription and translation.[43] The pH changes of the L929 cells treated with the cisplatin were also evaluated, and it suggested that minor pH changes occurred in the cisplatin-treated cells (Figure S21, Supporting Information, method 13), which would not affect the signal of the sensor. After the L929 cells were treated with the cisplatin, a turn from cyan to deep blue can be observed from the ratiometric images of most points of the SiNWs-FITC@SiO_2-20-Rho-100 that was incubated across the cells, indicating the decrease of the ATP levels at these points (Figure 6a). These results evidenced that the ATP levels of the cells reduced during the apoptosis, which was in accordance with the previous reports.[44,45] Combined with the confocal image (Figure 6b), the ATP level of the nucleus (green dots, Figure 6c) and cytoplasm (red dots, Figure 6c) can be determined at different times. We can find that a more obvious ATP decrease was exhibited in the nucleus compared with that in the cytoplasm (Figure 6d). Two more parallel experiments were performed, and the results presented in Table S3 also illuminated the above physiological process. A similar phenomenon was also observed in the cisplatin-treated HeLa cells (Figure S22). As cisplatin would induce cell apoptosis and result in the shortage of ATP in whole cells, understanding the behaviors of the ATP in the

https://doi.org/10.1021/acs.analchem.2c02030
Anal. Chem. 2022, 94, 11813−11820

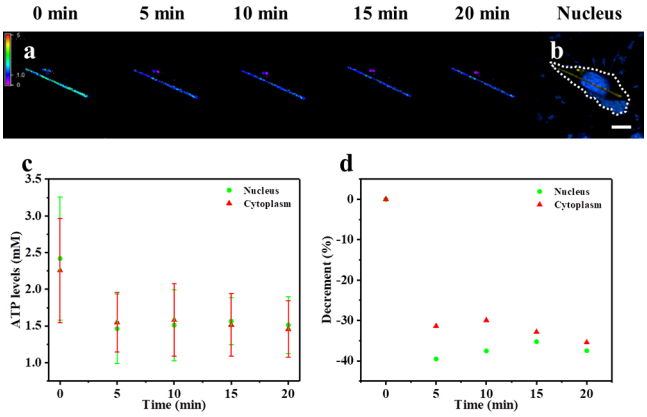

Figure 6. (a) Ratiometric images of the SiNWs-FITC@SiO_2-20-Rho-100 inside a single L929 cell treated with cisplatin (50 μM) for different times and (b) confocal image of the SiNWs-FITC@SiO_2-20-Rho-100 inside a single L929 cell (scale bar: 10 μm; ratio bar: 0−5). (c) Changes in the ATP levels of the nucleus (green dots, n = 37 points on the single sensor) and cytoplasm (red dots, n = 55 points on the single sensor) over time. (d) Decrements in the ATP levels of the nucleus and cytoplasm after the L929 cell was treated with cisplatin (the error bars represent the standard deviations based on the ATP levels at the points located in the cytoplasm and nucleus).

cells treated with cisplatin could refer to the above ATP change in the cells stimulated by the oligomycin. During cell apoptosis, the cells may protect themselves by preferentially lowering the ATP levels of the nucleus. These results above evidenced that the SiNWs-FITC@SiO_2-20-Rho-100 is capable of simultaneously monitoring the ATP fluctuation in the nucleus and cytoplasm during a cellular event.

CONCLUSIONS

In this work, we fabricated a nanowire-based ATP biosensor and realized simultaneous monitoring of the ATP levels of the nucleus and cytoplasm with a high spatial resolution. The as-fabricated ATP biosensor exhibited a ratiometric and reversible response to ATP and possessed a fine photo-stability and outstanding selectivity toward ATP. Employing the ATP biosensor, we simultaneously determined the ATP levels of cytoplasm and nucleus inside a single cell. It was found that the ATP level of the cytoplasm was 21 ± 8% lower than that of the nucleus in L929 cells, which was 32 ± 18% in HeLa cells. When treated with Ca^{2+}, the L929 and HeLa cells performed an increase of ATP levels, and the increments of the ATP level of the cytoplasm were higher than that of the nucleus. On the contrary, ATP decreased in both L929 and HeLa cells treated with oligomycin, and the decrement of the ATP level of the nucleus was higher than that of the cytoplasm. When the cell apoptosis was induced by cisplatin, the ATP decreased in both the cytoplasm and nucleus, and a higher decrement of the ATP level was occurred in the nucleus. The results achieved in this work would be beneficial to comprehensively elucidate the ATP-related cellular events. Moreover, apart from cell apoptosis, the ATP biosensor developed in this work can be employed to investigate more cellular events.

ASSOCIATED CONTENT

Supporting Information

The Supporting Information is available free of charge at https://pubs.acs.org/doi/10.1021/acs.analchem.2c02030.

Materials & instruments; experimental method; ^{1}H NMR and mass spectroscopy of the Rho-N_3H_5; SEM and TEM images of the SiNWs-FITC@SiO_2-20-Rho-100; XPS spectrum; uniformity, response time, and photo-stability of the SiNWs-FITC@SiO_2-20-Rho-100; and experiments in HeLa cells (PDF)

3D scanning (MP4)

AUTHOR INFORMATION

Corresponding Authors

Lixuan Mu − *Key Laboratory of Photochemical Conversion and Optoelectronic Materials, Technical Institute of Physics and Chemistry, Chinese Academy of Sciences, Beijing 100190, China;* orcid.org/0000-0002-6613-5368; Phone: +86-10-82543788; Email: mulixuan@mail.ipc.ac.cn

Wensheng Shi − *Key Laboratory of Photochemical Conversion and Optoelectronic Materials, Technical Institute of Physics and Chemistry, Chinese Academy of Sciences, Beijing 100190, China; University of Chinese Academy of Sciences, Beijing 100049, China; Ganjiang Innovation Academy, Chinese Academy of Sciences, Ganzhou 341000, China;* orcid.org/0000-0001-5747-4862; Phone: +86-10-82543513; Email: shiws@mail.ipc.ac.cn

Authors

Mingliang Mei − *Key Laboratory of Photochemical Conversion and Optoelectronic Materials, Technical Institute of Physics and Chemistry, Chinese Academy of Sciences, Beijing 100190, China; University of Chinese Academy of Sciences, Beijing 100049, China*

Yuan Wang − *Key Laboratory of Photochemical Conversion and Optoelectronic Materials, Technical Institute of Physics and Chemistry, Chinese Academy of Sciences, Beijing 100190, China; University of Chinese Academy of Sciences, Beijing 100049, China*

Sen Liang − *Key Laboratory of Photochemical Conversion and Optoelectronic Materials, Technical Institute of Physics and Chemistry, Chinese Academy of Sciences, Beijing 100190, China; University of Chinese Academy of Sciences, Beijing 100049, China*

Qiaowen Zhao − *Key Laboratory of Photochemical Conversion and Optoelectronic Materials, Technical Institute of Physics and Chemistry, Chinese Academy of Sciences, Beijing 100190, China; University of Chinese Academy of Sciences, Beijing 100049, China*

Lushan Huang − *Key Laboratory of Photochemical Conversion and Optoelectronic Materials, Technical Institute of Physics and Chemistry, Chinese Academy of Sciences, Beijing 100190, China; University of Chinese Academy of Sciences, Beijing 100049, China*

Guangwei She − *Key Laboratory of Photochemical Conversion and Optoelectronic Materials, Technical Institute of Physics and Chemistry, Chinese Academy of Sciences, Beijing 100190, China;* orcid.org/0000-0003-1017-5456

Complete contact information is available at: https://pubs.acs.org/10.1021/acs.analchem.2c02030

Notes

The authors declare no competing financial interest.

https://doi.org/10.1021/acs.analchem.2c02030
Anal. Chem. 2022, 94, 11813−11820

■ ACKNOWLEDGMENTS

This work was supported by the National Key R&D Program of China (2017YFE0196400), NSFC (52172107, 21975269), and Chinese Academy of Sciences (QYZDJ-SSW-JSC032, ZDRW-CN-2021-3-3, GJHZ201938).

■ REFERENCES

(1) Patel, A.; Malinovska, L.; Saha, S.; Wang, J.; Alberti, S.; Krishnan, Y.; Hyman, A. A. *Science* **2017**, *356*, 753−756.
(2) Hardie, D. G.; Ross, F. A.; Hawley, S. A. *Nat. Rev. Mol. Cell. Biol* **2012**, *13*, 251−262.
(3) Harvey, R. A.; Ferrier, D. R., *Biochemistry*. Fifth Edition ed.; Lippincott Williams & Wilkins: Philadelphia, 2011.
(4) Chandar, N.; Viselli, S., *Cell and Molecular Biology*. Lippincott Williams & Wilkins: Philadelphia, 2010.
(5) Zhang, J.; Goliwas, K. F.; Wang, W.; Taufalele, P. V.; Bordeleau, F.; Reinhart-King, C. A. *P. Natl. Acad. Sci. U.S.A.* **2019**, *116*, 7867−7872.
(6) Tantama, M.; Martinez-Francois, J. R.; Mongeon, R.; Yellen, G. *Nat. Commun.* **2013**, *4*, 2550−2560.
(7) Majdi, S.; Larsson, A.; Najafinobar, N.; Borges, R.; Ewing, A. G. *ACS Chem. Neurosci.* **2019**, *10*, 2459−2466.
(8) Zhao, D.; Chang, D.; Zhang, Q.; Chang, Y.; Liu, B.; Sun, C.; Li, Z.; Dong, C.; Liu, M.; Li, Y. *J. Am. Chem. Soc.* **2021**, *143*, 15084−15090.
(9) Budd, S. L.; Tenneti, L.; Lishnak, T.; Lipton, S. A. *Proc. Natl. Acad. Sci. U. S. A.* **2000**, *97*, 6161−6166.
(10) Miyoshi, N.; Oubrahim, H.; Chock, P. B.; Stadtman, E. R. *Proc. Natl. Acad. Sci. U. S. A.* **2006**, *103*, 1727−1731.
(11) Lin, M. T.; Beal, M. F. *Nature* **2006**, *443*, 787−795.
(12) Wang, L.; Yuan, L.; Zeng, X.; Peng, J.; Ni, Y.; Er, J. C.; Xu, W.; Agrawalla, B. K.; Su, D.; Kim, B.; Chang, Y. T. *Angew. Chem., Int. Ed.* **2016**, *55*, 1773−1776.
(13) Jun, Y. W.; Wang, T.; Hwang, S.; Kim, D.; Ma, D.; Kim, K. H.; Kim, S.; Jung, J.; Ahn, K. H. *Angew. Chem., Int. Ed.* **2018**, *57*, 10142−10147.
(14) Zhao, Y. T.; Chen, X. X.; Jiang, W. L.; Li, Y.; Fei, J.; Li, C. Y. *ACS Appl. Mater. Interfaces* **2020**, *12*, 47840−47847.
(15) Ren, T. B.; Wen, S. Y.; Wang, L.; Lu, P.; Xiong, B.; Yuan, L.; Zhang, X. B. *Anal. Chem.* **2020**, *92*, 4681−4688.
(16) Takei, Y.; Arai, S.; Murata, A.; Takabayashi, M.; Oyama, K.; Ishiwata, S.; Takeoka, S.; Suzuki, M. *ACS Nano* **2014**, *8*, 198−206.
(17) Bu, C.; Mu, L.; Cao, X. X.; Chen, M.; She, G. W.; Shi, W. S. *ACS Appl. Mater. Interfaces* **2018**, *10*, 33416−33422.
(18) Geng, X.; Sun, Y. Q.; Guo, Y. F.; Zhao, Y. M.; Zhang, K.; Xiao, L. H.; Qu, L. B.; Li, Z. H. *Anal. Chem.* **2020**, *92*, 7940−7946.
(19) Carling, D.; Mayer, F. V.; Sanders, M. J.; Gamblin, S. J. *Nat. Chem. Biol.* **2011**, *7*, 512−518.
(20) Bennett, N. K.; Nguyen, M. K.; Darch, M. A.; Nakaoka, H. J.; Cousineau, D.; Ten Hoeve, J.; Graeber, T. G.; Schuelke, M.; Maltepe, E.; Kampmann, M.; Mendelsohn, B. A.; Nakamura, J. L.; Nakamura, K. *Nat. Commun.* **2020**, *11*, 4319−4334.
(21) Yan, R.; Park, J. H.; Choi, Y.; Heo, C. J.; Yang, S. M.; Lee, L. P.; Yang, P. *Nat. Nanotechnol.* **2012**, *7*, 191−196.
(22) Ying, Y. L.; Hu, Y. X.; Gao, R.; Yu, R. J.; Gu, Z.; Lee, L. P.; Long, Y. T. *J. Am. Chem. Soc.* **2018**, *140*, 5385−5392.
(23) Gong, Z.; Wu, T.; Chen, X.; Guo, J.; Zhang, Y.; Li, Y. *Nano Lett.* **2021**, *21*, 1469−1476.
(24) Cao, X.; Mu, L.; Chen, M.; Bu, C.; Liang, S.; She, G.; Shi, W. *Adv. Biosyst.* **2018**, 1800213−1800219.
(25) Chen, M.; Mu, L.; Wang, S.; Cao, X.; Liang, S.; Wang, Y.; She, G.; Yang, J.; Wang, Y.; Shi, W. *ACS Chem. Neurosci.* **2020**, *11*, 1283−1290.
(26) Tan, K. Y.; Li, C. Y.; Li, Y. F.; Fei, J.; Yang, B.; Fu, Y. J.; Li, F. *Anal. Chem.* **2017**, *89*, 1749−1756.
(27) Mei, M.; Mu, L.; Liang, S.; Wang, Y.; She, G.; Shi, W. *Biosens. Bioelectron.* **2021**, *178*, 113025−113032.
(28) Hermanson, G. T., *Bioconjugate Chemistry*. Second Edition ed.; Elsevier: 2008.
(29) Jeske, M.; Jung, K. G.; Schultze, J. W.; Thonissen, M.; Munder, H. *Surf. Interface Anal.* **1994**, *22*, 363−366.
(30) Finster, J. *Vacuum* **1990**, *41*, 1586−1589.
(31) Cauzzi, D.; Marzolini, G.; Predieri, G.; Tiripicchio, A.; Costa, M.; Salviati, G.; Armigliato, A.; Basini, L.; Zanoni, R. *J. Mater. Chem.* **1995**, *5*, 1375−1381.
(32) Nakagaki, R.; Frost, D. C.; Mcdowell, C. A. *J. Electron. Spectros. Relat. Phenomena* **1981**, *22*, 289−296.
(33) Kallury, K. M. R.; Debono, R. F.; Krull, U. J.; Thompson, M. *J. Adhes. Sci. Technol.* **1991**, *5*, 801−814.
(34) Liu, J. H.; Li, D. Y.; He, J. H.; Yuan, D.; Li, R. S.; Zhen, S. J.; Li, Y. F.; Huang, C. Z. *ACS Appl. Mater. Interfaces* **2020**, *12*, 4815−4820.
(35) Han, F.; Xu, Y.; Jiang, D.; Qin, Y.; Chen, H. *Anal. Biochem.* **2013**, *435*, 106−113.
(36) Matsuyama, S.; Llopis, J.; Deveraux, Q. L.; Tsien, R. Y.; Reed, J. C. *Nat. Cell Biol.* **2000**, *2*, 318−325.
(37) Lagadic-Gossmann, D.; Huc, L.; Lecureur, V. *Cell. Death. Differ.* **2004**, *11*, 953−961.
(38) Zheng, J.; Li, X.; Wang, K.; Song, J.; Qi, H. *Anal. Chem.* **2020**, *92*, 10940−10945.
(39) Zheng, X.; Peng, R.; Jiang, X.; Wang, Y.; Xu, S.; Ke, G.; Fu, T.; Liu, Q.; Huan, S.; Zhang, X. *Anal. Chem.* **2017**, *89*, 10941−10947.
(40) Griffiths, E. J.; Rutter, G. A. *Biochim. Biophys. Acta, Bioenerg.* **2009**, *1787*, 1324−1333.
(41) Zeng, F.; Tang, L.; Zhang, Q.; Shi, C.; Huang, Z.; Nijiati, S.; Chen, X.; Zhou, Z. *Angew. Chem., Int. Ed.* **2021**, No. e202112925.
(42) Huang, B.; Geng, Z.; Yan, S.; Li, Z.; Cai, J.; Wang, Z. *Anal. Chem.* **2017**, *89*, 8816−8821.
(43) Florea, A. M.; Busselberg, D. *Cancers* **2011**, *3*, 1351−1371.
(44) Deng, J. J.; Wang, K.; Wang, M.; Yu, P.; Mao, L. Q. *J. Am. Chem. Soc.* **2017**, *139*, 5877−5882.
(45) Wang, K.; Qian, M.; Qi, H.; Gao, Q.; Zhang, C. *Nanoscale* **2020**, *12*, 15663−15669.

https://doi.org/10.1021/acs.analchem.2c02030
Anal. Chem. 2022, 94, 11813−11820